Chemical Papers
https://doi.org/10.1007/s11696-026-04973-5

ORIGINAL PAPER

KOH-activated carbon from *Aframomum angustifolium* fruit shells for caffeine removal from aqueous solution

Baraka Alfaksad Kasazi[1] · **Alinanuswe Joel Mwakalesi**[1] · **Emmy Solomon Lema**[1]

Received: 12 December 2025 / Accepted: 28 April 2026

Abstract
This study reports on the preparation of activated carbon using *Aframomum angustifolium* fruit shells (FPAA) and its application for the removal of caffeine from aqueous solution. The activated carbon was prepared using KOH activation in a 1:2 ratio, followed by pyrolysis at 500 °C for 1 h. The activated carbon (AC-K) was characterized using the point of zero charge of potential of hydrogen (pHpzc), N_2 adsorption–desorption analysis, scanning electron microscopy–energy-dispersive X-ray spectroscopy (SEM–EDX), X-ray diffraction (XRD), and Fourier transform infrared spectroscopy (FTIR). The surface of AC-K exhibited a mesoporous structure with an increased BET surface area from 335 to 407.6 m^2/g. The classical method and response surface methodology (RSM) using Box–Bohnken design (BBD) were used to optimize the performance of AC-K to remove caffeine from aqueous solutions. The results indicated that the adsorption aligned best with the Langmuir model ($R^2 = 0.996$ and RMSE = 0.3531), indicating the formation of a monolayer film. In addition, the adsorption was described by the pseudo-second-order model ($R^2 = 0.995$ and RMSE = 0.017). The highest caffeine removal efficiencies were 78.67 and 90.40% as determined using classical and BBD methods, respectively. Therefore, the preparation and use of an eco-friendly and previously unexplored precursor for activated carbon preparation is demonstrated in the current study. This study contributes to sustainable waste valorization while offering a promising alternative material for the removal of emerging contaminants such as caffeine from water systems.

Keywords *Aframomum angustifolium* · Fruit shells · Activated carbon · Caffeine

Introduction

Caffeine (1,3,7-trimethylxanthine) is an emerging environmental contaminant, largely due to its extensive use in pharmaceuticals, beverages, and personal care products (Korekar et al. 2020). It is naturally present in over 60 plant species like coffee, tea, and cocoa (Reddy et al. 2024). The industrial caffeine production is rising to meet growing global demand (Korekar et al. 2020) as approximately 80% of the world's population consumes caffeine daily (Samoggia and Rezzaghi 2021). However, 1–5% of consumed caffeine is excreted in unchanged form (Yang et al. 2025). Consequently, they enter into aquatic environments like rivers, lakes, oceans, and groundwater (Li et al. 2020b). Caffeine may bio-accumulate in living organisms in aquatic environments and cause negative impacts due its toxic nature at high doses (Rodrigues et al. 2025). The effects of caffeine residues such as altered swimming and feeding patterns, as well as increased mortality rates, were reported in Zebrafish (Teixeira et al. 2025). Additionally, the development of abnormalities in the cardiovascular, nervous and neuromuscular systems of Zebrafish embryos and larvae have been observed (Clayman and Connaughton 2022). Therefore, the removal of caffeine from the aqueous environment is highly needed.

Conventional treatment techniques for the removal of caffeine from aqueous systems have been widely investigated (Rigueto et al. 2020; Rathinam et al. 2026). The techniques that have been reported include biological processes, chemical processes (advanced oxidation, flocculation-flocculation), and physical processes (membrane filtration) (Toniciolli Rigueto et al. 2020). Biological treatments, such as activated sludge systems, can partially degrade caffeine;

✉ Baraka Alfaksad Kasazi
baraka.kasazi@sua.ac.tz

[1] Department of Chemistry and Physics, College of Natural and Applied Sciences, Sokoine University of Agriculture, P.O. Box 3038, Morogoro, Tanzania

however, they are often limited by long retention times and incomplete removal, especially at higher concentrations (Toniciolli Rigueto et al. 2020). Advanced oxidation processes such as ozonation and photocatalysis, can achieve high degradation efficiencies; however, they are associated with high operational costs, energy demand, and the potential formation of toxic by-products (Babuponnusami et al. 2023). Membrane-based technologies, such as nanofiltration and reverse osmosis, provide high removal efficiencies but they suffer from membrane fouling, high maintenance costs, and concentrate disposal (Abdulsalam et al. 2025). Similarly, coagulation–flocculation methods are generally inefficient for removing low-molecular-weight and highly soluble compounds like caffeine. Thus, the adsorption has emerged as a promising alternative in removing micropollutants from water. It is regarded as one of the most effective methods for water remediation due to its operational simplicity, effectiveness, and versatility in utilizing a broad spectrum of adsorbent materials (Tran 2023).

Activated carbon (AC) is one of the highly effective adsorbents due to its extensive porous network and large surface area (Sharma et al. 2022). However, the commercial AC from non-renewable sources, such as coals, lignite, peat and petroleum pitch is expensive because its production requires high energy (800–1000 °C) (Neolaka et al. 2023). Thus, the development of alternative and cost-effective methods for the production of AC from plant-sourced biomass has attracted recent research attention. Consequently, the use of abundant biowastes such as mango peels, nutshells, and straw for the preparation of activated carbon has been reported (Ramutshatsha-Makhwedzha et al. 2022; Dao and Le Luu 2020). The conversion of biowastes into AC directly addresses the management of biowastes and provides a sustainable solution to water treatment (Ullah et al. 2024).

The plant species *Aframomum angustifolium* produces fruits that are consumed as food in several African countries, including the Democratic Republic of Congo, Tanzania, and Uganda (Kyayesimira et al. 2019; Tugume and Research 2020). Following the consumption, the fruit shells are typically disposed of as waste in landfills. The accumulation of this biowaste presents a growing environmental challenge, as its natural decomposition in landfills releases greenhouse gases such as methane that contribute to global warming (Sri Shalini et al. 2021). Like many other forestry and agricultural biowastes, these fruit shells are composed of lignocellulose, primarily cellulose, hemicellulose, and lignin (Parmar 2017). This chemical composition is suitable for the preparation of AC, as it provides a robust carbonaceous framework that can be converted into a highly porous structure. However, there is limited information on the use of AC from *A. angustifolium* fruit shells and its application for the adsorption of caffeine from aqueous solutions. Therefore, this study aimed to address this research gap by attempting to prepare activated carbon from the biowaste and investigate its performance for the removal of caffeine from aqueous solutions.

Optimization plays a crucial role in improving process efficiency, reducing energy consumption and maximizing profit (Saghir et al. 2025; Zhang et al. 2023). Therefore, different conventional methods have been employed to determine the effect of individual factors on process outcomes. Most of these methods are simple to apply; however, they are often time-consuming, resource-intensive, and unable to capture interactive effects among variables (Azeez et al. 2022a). In contrast, statistical optimization techniques based on the response surface methodology (RSM) offer a systematic and efficient means of evaluating the combined effects of multiple parameters simultaneously. They are based on the application of the factorial design to establish optimum experimental conditions. Among RSM designs, the Box–Bohnken Design (BBD) has gained significant attention due to a reduced number of experimental runs and effective modelling of quadratic responses without requiring extreme factor level combinations (Azeez et al. 2022b). The method is helpful for the simultaneous study of the experimental factors, optimization and interactions to determine the influence of multiple factors on the properties of interest. Therefore, the application of RSM-BBD ensures robust process modelling and enhances the reliability of predicted optimum conditions (Adetokun et al. 2018). In the current study, the conventional and RSM-BBD methods were applied to optimize factors such as pH, adsorbent dosage, initial caffeine concentration, and adsorption time to achieve optimal caffeine removal efficiency.

Materials and methods

Materials

Aframomum angustifolium fruits were collected from Kasulu District, located in Kigoma Region, Tanzania.

Chemicals

Potassium hydroxide, KOH (85%) from Loba Chemie, Mumbai, India, sodium dihydrogen orthophosphate, $NaH_2PO_4 \cdot 2H_2O$ (98%) from a Fisher Scientific International Company, di-sodium hydrogenphosphate-2-hydrate, $Na_2HPO_4 \cdot 2H_2O$ (99.5%) from Riedel-deHaën, ethanol, CH_3CH_2OH from Scharlau Chemical Company in Spain, sodium hydroxide, NaOH (97%), sodium chloride, NaCl (99.5%), hydrochloric acid (37%) and caffeine from Loba

Chemie PVT Ltd, 107 Wodehouse Road, Mumbai 400005 India were used in this study.

Instrumentation

Muffle furnace from Medlab Scientific Equipments, Mumbai, India ,Oscillating water bath from Sheldon manufacturing, inc.300 N.26th CORNELIUS, OR97113, Porosity analyzer, Quantachrome NovaWin©1994-2013, Quntachrome Instruments V11.03, 6715 UV/Vis Spectrophotometer (JENWAY), X-ray diffraction (Malvern Analytical Aeris Benchtop XRD), Scanning electron microscope (JOEL, JSM-6610LV), and IRAffinity-1S Fourier transform infrared spectrophotometer-SHIMADZU.

Sample preparation

The sample preparation was performed following the reported procedures (Kasazi et al. 2026). Briefly, *A. angustifolium* fruits were washed, peeled, and sun-dried for 1 week. The dried shells were ground into a fine powder using a blender, sieved (125 µm mesh), and stored in polyethylene bags.

Preparation of AC

The preparation of AC followed the previously established protocol with minor modifications (Chagu and Mwakalesi 2026). The shell powder (FPAA) and potassium hydroxide (KOH) were mixed at an impregnation ratio of 1:2 (30 g FPAA: 60 g KOH). The mixture was soaked in 600 mL of distilled water for 24 h and then filtered using Whatman filter paper (125 mm diameter). The collected solid sample was transferred to a crucible, and dried in an oven at 110 °C for 36 h. The dried material was carbonized at 500 °C for 1 h to produce KOH-activated carbon (AC-K) that was allowed to cool for 1 h. The AC-K was then ground and soaked in 500 mL of a 20% ethanol–water solution for 3 h, and filtered. The collected AC-K was then resoaked in 500 mL of 0.1 M hydrochloric acid (HCl) solution for 1 h to neutralize basic residues. The AC-K was then washed repeatedly with distilled water until the wash water reached a stable pH of 7. The washed AC-K was dried in an oven at 105 °C for 12 h and allowed to cool. Finally, the AC-K was ground and resultant powder stored in a vial wrapped in a polyethylene bag for subsequent use.

Characterization of AC

Surface area analysis was performed using the BET method (Quantachrome NovaWin® v11.03, Quantachrome Instruments). The functional groups of FPAA (precursor) and AC-K were analyzed using FTIR spectroscopy (Shimadzu IRAffinity-1S). For this, approximately 2.0 mg of the sample was mixed with 0.1 g KBr using a mortar and pestle, compressed into pellets, and analysed using the FTIR instrument. The surface morphology and elemental composition of FPAA and AC-K were examined using scanning electron microscopy coupled with energy-dispersive X-ray spectroscopy (JEOL JSM-6610LV SEM). The 100 mg of sample was put on a clean aluminium stub with carbon tape using a clean spatula. The stub was then placed in a sputter coater with Pd/Au at a current of 20 A for 60 s. Then, the stub was transferred to the SEM/EDS stage, secured, and pumped down to the vacuum. The phase structure and graphitic properties of FPAA and AC-K were analyzed using an X-ray diffractometer (Malvern Panalytical Aeris Benchtop XRD). The sample was further powdered to 10 µm and mounted to the sample holder provided by Aeris system, and levelled using a glass slide. The sample was then inserted in the X-ray tube (Cu-Kα, λ = 1.5415 Å) of the XRD machine and then scanned at 2θ range of 5°–90°. The zero point charge pH (pHpzc) was determined by the pH drift method as previously described (Mpaka and Mwakalesi 2025). Briefly, solutions with different pH ranging from 2 to 12 were prepared using 0.1 M NaCl as background electrolyte, with pH adjusted using 0.1 M HCl or 0.1 M NaOH. The AC-K (50 mg) was added to 40 mL aliquots of each pH solution and shaken for 24 h at an agitation speed of 100 rpm and 25 °C. Thereafter, the mixtures were filtered for the determination of the final pH. The plot of final pH versus initial pH was constructed to obtain the equilibrium pH that reflects a zero charge pH (pHpzc).

Adsorption experiment

The adsorption experiments were performed in batch mode by suspending the appropriate mass of adsorbent (20–120 mg) in 5 mL of aqueous caffeine solutions of concentrations (20–600 mg/L). The mixture was then placed in a water bath and agitated at 100 rpm. During the process, sample aliquots were withdrawn at regular intervals. The caffeine concentration in these aliquots was quantified by measuring the absorbance at 276 nm using a UV–Vis spectrophotometer (Rzyska-Szczupak et al. 2025). The performance was evaluated using removal efficiency (%) and equilibrium adsorption capacity (Q) determined using Eqs. 1 and 2.

$$R(\%) = \left(\frac{C_o - C_e}{C_o}\right) \times 100 \tag{1}$$

$$Q_e = \frac{C_o - C_e}{m} \times V \tag{2}$$

where R is the removal efficiency of caffeine (%), C_o (mg/L) is the initial concentration of caffeine (mg/L), C_e (mg/L) is the concentration of caffeine at equilibrium, Q_e (mg/g) is the adsorption capacity, m (g) is the mass of AC, and V (L) is the volume of caffeine solution.

Results and discussion

Characterization of AC-K adsorbent

N_2 adsorption–desorption analysis

Surface area of AC-K was characterized using the N_2 adsorption–desorption analysis. The BET surface area of AC-K increased to 408 m^2/g from 336 m^2/g of the precursor, FPAA (Table 1). The observed increase in the surface area was possibly caused by the removal of volatile compounds to create a highly porous AC. This thermal decomposition releases gases like CO and CO_2, tearing open the internal structure of the material to develop pores (Tihay and Gillard 2010). The process, often enhanced by high temperatures and chemical agents, leaves behind a carbon skeleton with vastly increased surface area. The temperature of (500 °C) was used for the activation process performed in the current study as the temperature greater than 500 °C produced low yield. Furthermore, the total pore volume increased from 1.186 to 1.880 cm^3/g, while the average pore diameter increased from 0.605 to 0.682 nm. The pore volume increased from 0.292 to 0.390 cm^3/g, and the pore surface area increased from 185.874 to 240.480 m^2/g. The observed increase in the total pore volume and pore volume aligns with findings reported for the preparation of activated carbon using cashew nut shell biomass (Fonseca-Bermúdez et al. 2024). The significant increases in BET surface area, total pore volume, average pore size, pore volume, and pore surface area in AC-K compared to FPAA demonstrate its suitability as an effective adsorbent.

The findings for the N_2 adsorption–desorption isotherm (Fig. 1a, b) showed that the FPAA and AC-K exhibited a type IV adsorption–desorption isotherm, demonstrating the presence of a mesoporous structure (Guan et al. 2024). Similarly, the pore size distribution of the AC-K, as presented in Fig. 1c (BJH) and Fig. 1d (DFT), indicated the presence of mesopores. A similar AC with mesopores prepared using a mixture of rice husk and beet sugar was also reported (Kumagai et al. 2013). The mesoporous structure improves the rate of adsorption by facilitating faster diffusion of larger molecules (Valencia et al. 2019). Therefore, the mesoporous structure is a possible indicator that the prepared activated carbon is a versatile adsorbent for the removal of various contaminants.

Table 1 BET surface, total pore volume, average pore size, pore volume, pore diameter, and pore surface area of FPAA and AC-K

Type of material	BET surface area (m^2/g)	Total pore volume (cm^3/g)	Average pore size (nm)	BJH pore volume (cm^3/g)	BJH pore diameter (nm)	BJH pore surface area (m^2/g)
FPPA	335.809	1.186	0.522	0.292	3.391	185.874
AC-K	407.645	1.880	0.682	0.390	3.374	240.480

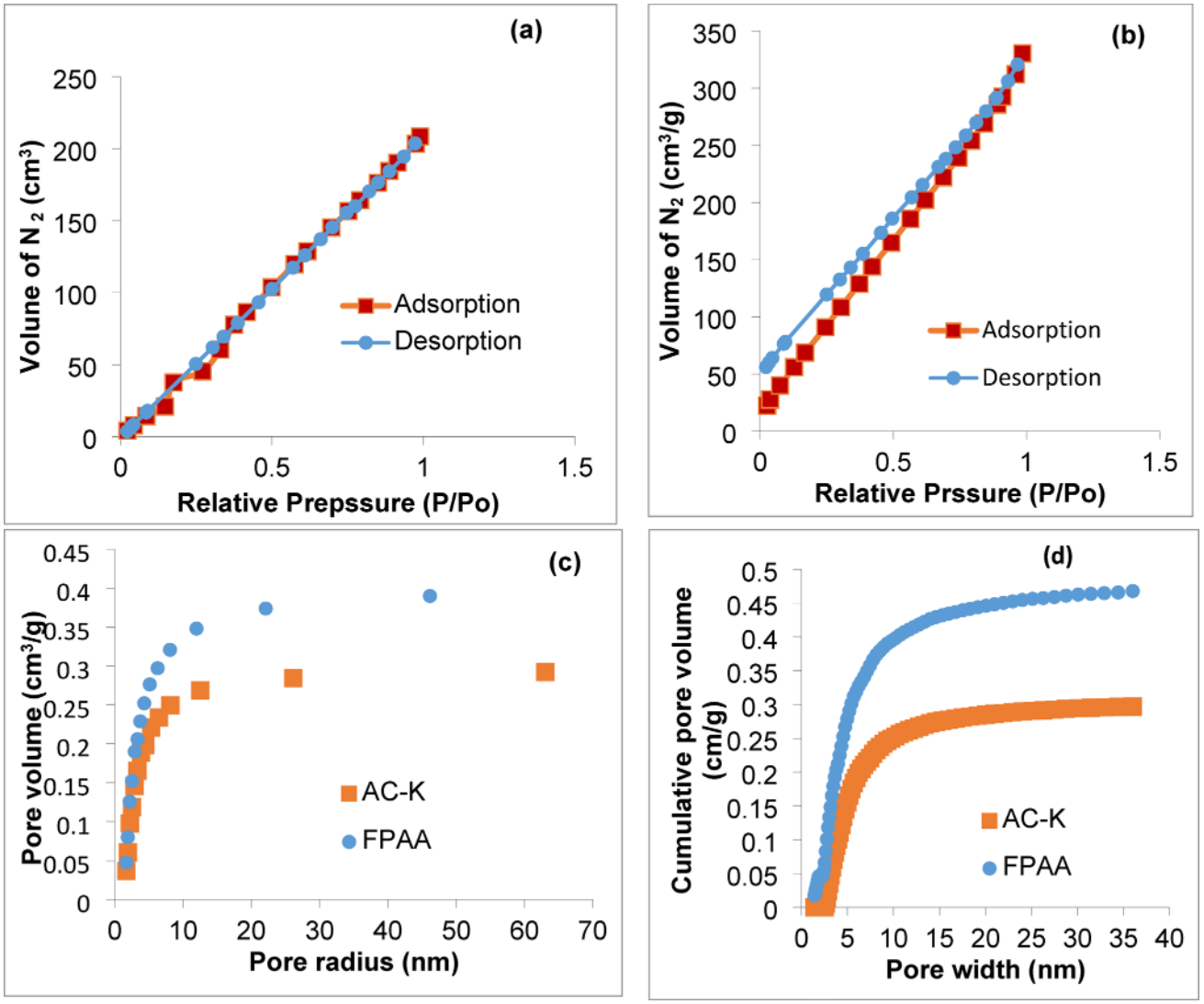

Fig. 1 Adsorption–desorption isotherms of FPAA (**a**) and AC-K (**b**) with BJH pore size distribution (**c**) and DFT pore size distribution (**d**)

SEM–EDX analysis

Scanning electron microscopy (SEM) was employed to analyze the morphological changes that occurred during the activation processes. The findings (Fig. 2a) showed that the precursor material (FPAA) exhibited a relatively smooth surface with no observable porosity. However, the surface of AC (Fig. 2b) displayed a highly textured surface with distinct, randomly distributed pores. This enhanced porosity is possibly attributed to structural modifications induced by KOH chemical activation and subsequent pyrolysis. During pyrolysis, KOH acts as a dehydrating agent, promoting the decomposition of the lignocellulosic framework and the release of volatile matter. Concurrently, it reacts with carbon atoms in a series of redox reactions, which actively etch the carbon matrix. This corrosive action creates mostly mesopores and widens existing pores, while the subsequent release of gaseous products (such as H_2 and CO) upon further heating contributes to the development of a highly porous and high surface area structure. The observed transformation from a relatively smooth to a roughened, porous morphology aligns with findings previously reported (Ibrahim et al. 2024). Thus, the generated porosity provides the extensive surface area and active sites necessary for the adsorption process.

The elemental composition of the FPAA (Table 2 and Fig. S1) and the AC-K (Table 2 and Fig. S2) provides direct evidence of the chemical transformations induced by the activation process. The analysis revealed a significant enrichment in carbon content alongside a sharp decline in oxygen content within the AC-K sample. This inverse relationship is an indicator of the successful carbonization and activation. The process facilitates a series of dehydration, decarboxylation, oxidation and dehydrogenation reactions,

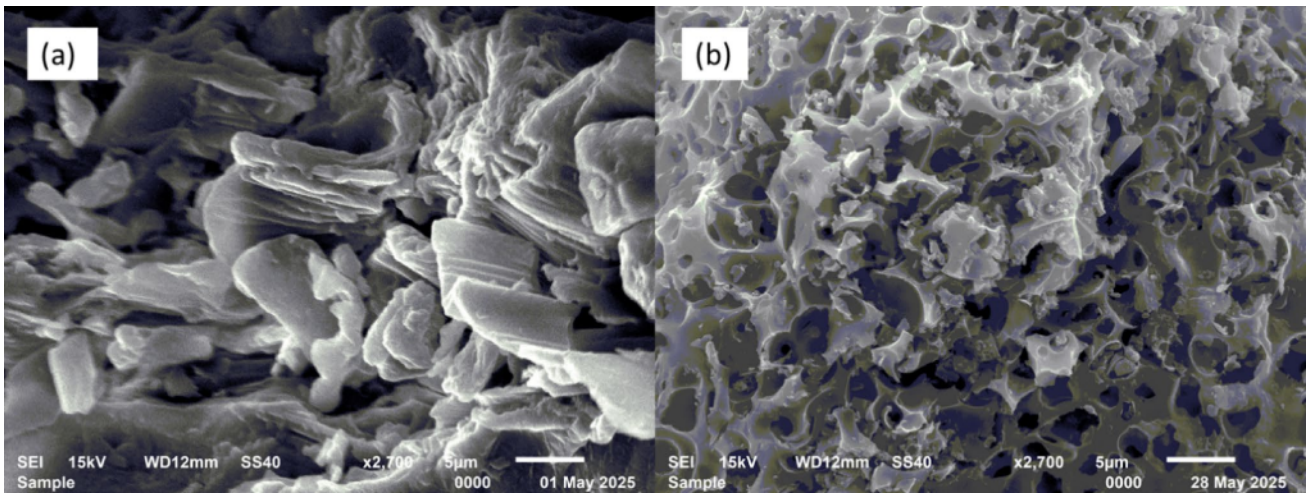

Fig. 2 SEM images **(a)** FPAA **(b)** AC-K

Table 2 Elemental compositions of FPAA and AC-K

Element	Weight % of FPAA	Weight % of AC-K
C	49.96	84.53
O	46.72	14.31
N	2.07	–
Na	–	0.01
Mg	0.49	0.53
P	0.18	–
Cl	–	0.06
K	0.45	0.07
Ca		0.05
Fe	0.05	–
Mn	0.06	–

which cleave and remove heteroatoms (O, H, N) in the form of volatile gases like H_2O, CO, CO_2, NO_2, NO and CH_4 (Durak et al. 2026). Reports indicated that cellulose, hemicellulose and lignin components of the precursor materials decompose during the pyrolysis process (Tan et al. 2015). The removal of non-carbon elements is linked to the development of the material's porosity. As these volatile compounds are expelled, they create a network of pores within the carbon matrix that increases the surface area. Consequently, the changes observed correlate with the development of the highly porous structure that determines the effectiveness of activated carbon.

XRD analysis

The structural changes introduced during the development of the activated carbon were analyzed using X-ray diffraction (XRD). The results (Fig. 3) indicated that the FPAA spectrum exhibits broad peaks at $2\theta \approx 20°$, 35° and 43°, while AC-K shows peaks at $2\theta \approx 15°$, 24° and 43°. The peak at $2\theta \approx 24°$ in AC-K corresponds to the (002) diffraction plane of graphitic carbon, indicating the development of graphite-like layered structures or an enhanced stacking order within carbon sheets (Nandi et al. 2023). The peak at $2\theta \approx 43°$ for AC-K represents the (100) plane of graphitic carbon. This peak is broader and less intense in both materials, reflecting a disordered carbon structure. Its persistence in AC-K suggests partial graphitization or alignment of aromatic rings occurred during activation (Mohite et al. 2024). The shift of the broad diffraction feature from $2\theta \approx 20°$ in FPAA to $2\theta \approx 15°$ and 24° in AC-K indicates an increase in the interlayer spacing between graphitic sheets resulting from the activation process (Minakshi et al. 2024). The broad nature of all observed peaks confirms that AC-K possesses predominantly amorphous character (Phuoc et al. 2023).

FTIR analysis

The FTIR results (Fig. 4) showed that the FPAA spectrum exhibits characteristic peaks at 1029 cm^{-1} and 1251 cm^{-1} (C–O), 1381 cm^{-1} (CH_3 or N=O), 1610 cm^{-1} (C–N), 1724 cm^{-1} (C=O), 2980 cm^{-1} (C–H stretch), 3344 cm^{-1} (O–H), and 3658 cm^{-1} (free O–H) (Megherbi et al. 2025; Pavia et al. 2001). In contrast, the AC-K FTIR spectrum showed the disappearance of the broad O–H peak at 3344 cm^{-1} , indicating the possible removal of oxygen-containing groups through dehydration or decarboxylation that occured during the activation. The disappearance of peaks at 2980 cm^{-1} (C–H), 3344 cm^{-1} (O–H of alcohol, phenol), and 3660 cm^{-1} (free O–H) was also observed. The observed disappearance was due to thermal degradation during the pyrolysis and reactions caused by KOH. The AC-K showed appearance a new peak at 1583 cm^{-1} (C=C) and retained a peak with reduced intensity at 1029 cm^{-1} (C–O) due to a new bonding environment. The similar peaks were previously reported in rice husk biochar (Miotto et al. 2024).

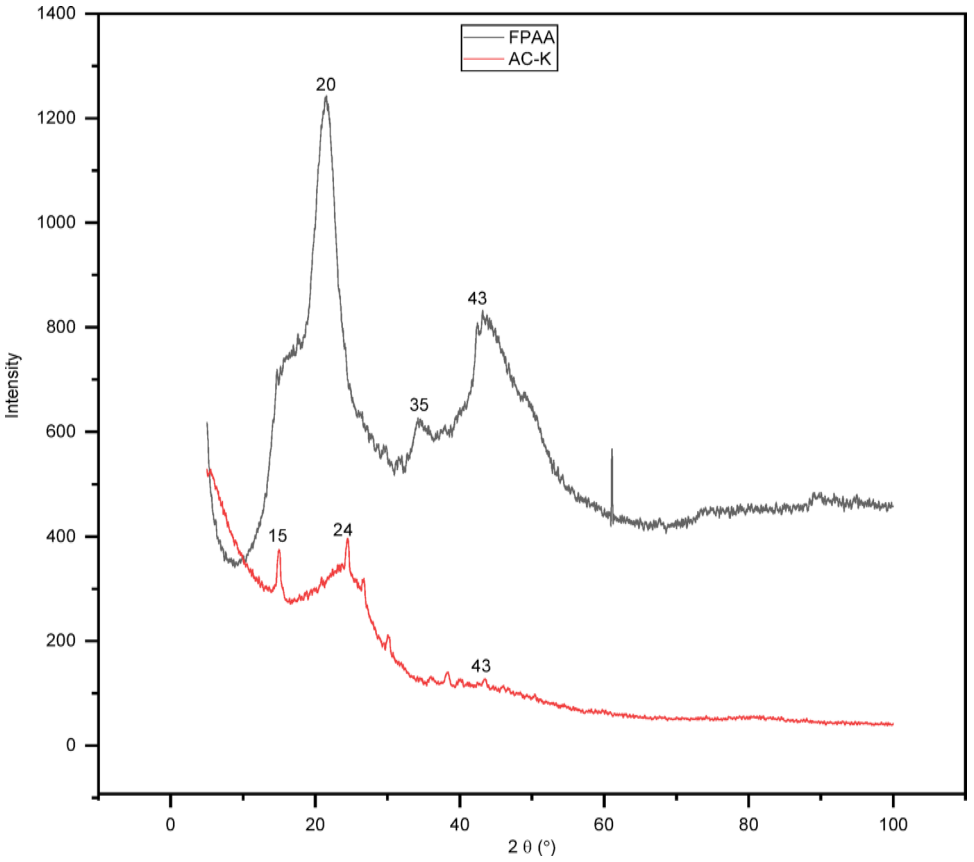

Fig. 3 XRD graphs for FPAA and AC-K

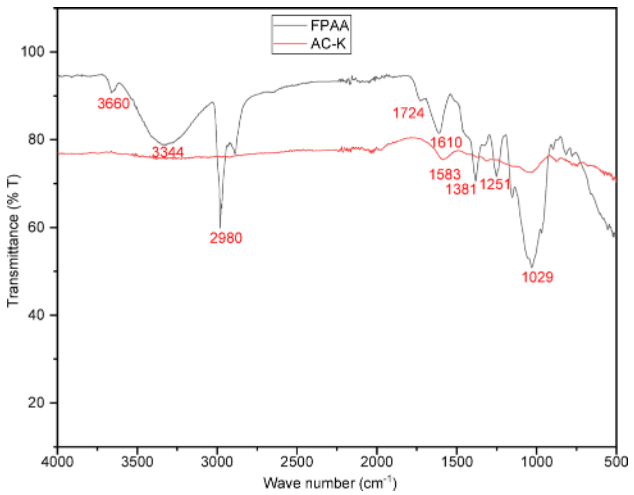

Fig. 4 FTIR results for FPAA and AC-K

Adsorption study

Effect of pH

The solution pH influences the adsorption process by affecting both the adsorbent surface charge and adsorbate speciation. The zero point charge pH of AC-K was determined as 6.0 (Fig. 5b), indicating a neutral surface charge at this pH. Below pHpzc, AC-K carries a net positive charge; above, it becomes negatively charged. As shown in Fig. 5a, the caffeine removal efficiency and adsorption capacity by AC-K increased from 50.87% and 0.5 mg/g at pH 2–68.22% and 0.68 mg/g at pH 7, and 70.19% and 0.7 mg/g at pH 8. This trend is likely to be attributed to the increased interaction between the AC-K surface and caffeine molecules (neutral at pH 3–8). Thus, the hydrogen bonding, π–π-interactions, Van Der Waal forces (dipole–dipole interactions and London dispersion forces), and pore filling are likely to be involved in the adsorption process. The possible hydrogen bonding between caffeine and AC-K is supported by the presence of a functional group (C–O bond) at 1029 cm^{-1} for either alcohol, ester, ether, anhydride, or carboxylic group on the FTIR spectrum for AC-K (Fig. 3 and Table S1). The adsorption of caffeine using a similar nature of interactions was also reported by others (Mahgoub et al. 2024). Though the highest removal (70.19%) and adsorption capacity (0.7 mg/g) occurred at pH 8, pH 7 (68.22% and 0.68 mg/g) was selected as optimal for environmental relevance, as most natural waters exhibit near-neutral pH. The selection of a similar pH for the adsorption of caffeine as in this study was reported in a previous study (Mahgoub et al. 2024).

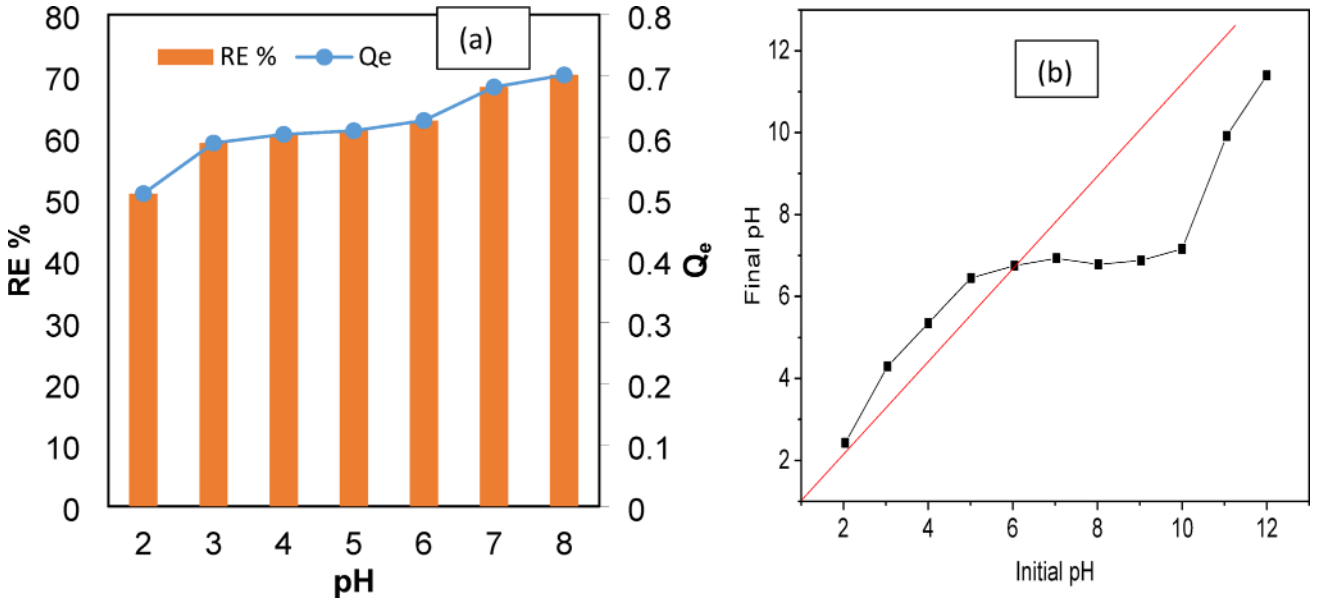

Fig. 5 Effect of pH on the adsorption of caffeine. Experimental conditions: Solution pH (2–8), dosage of adsorbent (20 g/L), initial concentration of caffeine (20 mg/L), solution temperature (298 K), agitation speed (100 rpm) and contact time (1 h) (**a**) with point of zero charge (pHpzc) of AC-K (**b**)

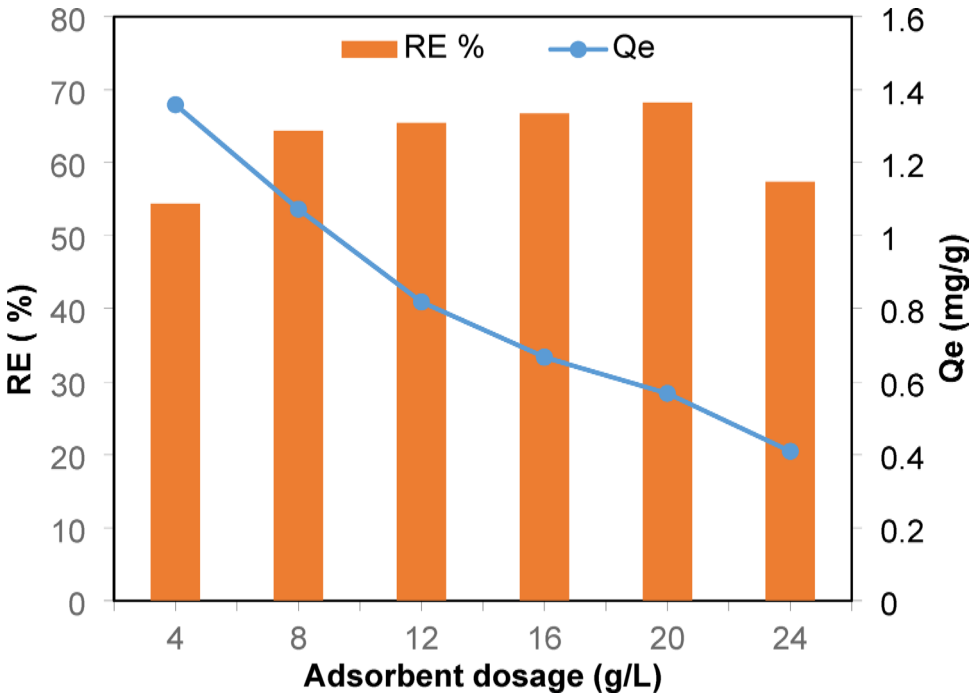

Fig. 6 Effect of dosage of adsorbent on the adsorption of caffeine. Experimental conditions: Solution pH (7), initial concentration (20 mg/L) of caffeine, temperature (298 K), agitation speed (100 rpm) and contact time (1 h)

Effect of adsorbent dosage

The influence of AC-K adsorbent dosage on caffeine removal efficiency is shown in Fig. 6. Increasing AC-K dosage from 4 to 20 g/L enhanced removal efficiency from 54.35 to 68.22%, attributed to greater availability of active adsorption sites. However, further dosage increases beyond 20 g/L resulted in slightly diminished efficiency (57.18% at 24 g/L), likely due to particle aggregation causing reduced site accessibility (Rahmawati et al. 2024). The increase in the removal efficiency is possibly attributed to increased adsorption sites due to increased dosage of AC (Alawa et al. 2025). Conversely, the adsorption capacity of caffeine using AC-K decreased as the adsorbent dosage increased from 1.358 mg/g at 4 g/L to 0.409 at 24 g/L adsorbent dose. This was due to too much adsorbent, which led to a reduction in caffeine amount per unit mass of adsorbent. The similar findings on the increase of removal efficiency and decrease

in adsorption capacity as dosage increased were previously reported on the adsorption of methyl orange and methylene blue using activated bio-carbon made from birchwood (Lee et al. 2024) and the adsorption of methylene blue using oak charcoal-based activated carbon (Kouhi et al. 2023).

Effect of initial concentration

The effect of initial caffeine concentration on removal efficiency and adsorption capacity using AC-K is shown in Fig. 7. The results showed that the removal efficiency increased as the initial concentration of caffeine increased up to an optimal concentration. The maximum removal efficiency (78.67%) occurred at 100 mg/L. Beyond this threshold, a decrease in efficiency was observed. The observed increase in the removal efficiency was possibly attributed to increased driving force for adsorption and more molecules to interact with the adsorbent's active sites. However, as the initial concentration becomes too high, the adsorption efficiency can decrease because the adsorbent's limited active sites become saturated, making it unable to adsorb all the available molecules (Banerjee and Chattopadhyaya 2017). This trend aligns with Rahmawati et al. (2024), who reported similar concentration-dependent behaviour during the removal of ceftriaxone and ciprofloxacin using corn cob-derived graphene oxide (Rahmawati et al. 2024). In both studies, the removal efficiency increased with concentration until reaching a saturation point. In contrast, the adsorption performance of caffeine using AC-K increased as the initial concentration increased. A similar finding related to an increase in removal efficiency up to a certain threshold and an increase in adsorption capacity without a threshold level on the adsorption of caffeine was previously reported using multi-wall carbon nanotube (Bahrami et al. 2017).

Adsorption isotherm

The Langmuir, Freundlich, and Temkin isotherm models were studied to evaluate the nature of the adsorption process. The experimental data were fitted to nonlinear isotherm equations (Table 3) to determine model adherence. As shown in Table 3 and Fig. 8, the adsorption of caffeine onto AC-K conformed to the Langmuir model, as its R^2 value is close to 1 (0.996) compared to that of Freundlich (0.951) and Temkin models (0.946). Also, the root mean square error (RMSE) value (Eq. 3) for Langmuir was lower (0.3531) compared to RMSE values for Freundlich (1.7719) and Temkin model (0.6376), further confirming the best fit of Langmuir model and 0.951 for Freundlich. The observations indicate that the adsorption process involves the formation of a monolayer film, with no interaction between adsorbed caffeine molecules. The maximum adsorption capacity of 22.02 mg/g obtained from the fitted model (Langmuir). The adsorption capacity reflects favorable interaction between caffeine molecules and the AC-K surface, primarily through π -π-interactions, hydrogen bonding, Van Der Waal forces (dipole–dipole interactions and London dispersion forces) and pore filling. A similar finding on fitting to the Langmuir model was previously reported on the adsorption of caffeine and acetaminophen adsorption using biomass-derived activated carbon (Melliti et al. 2024).

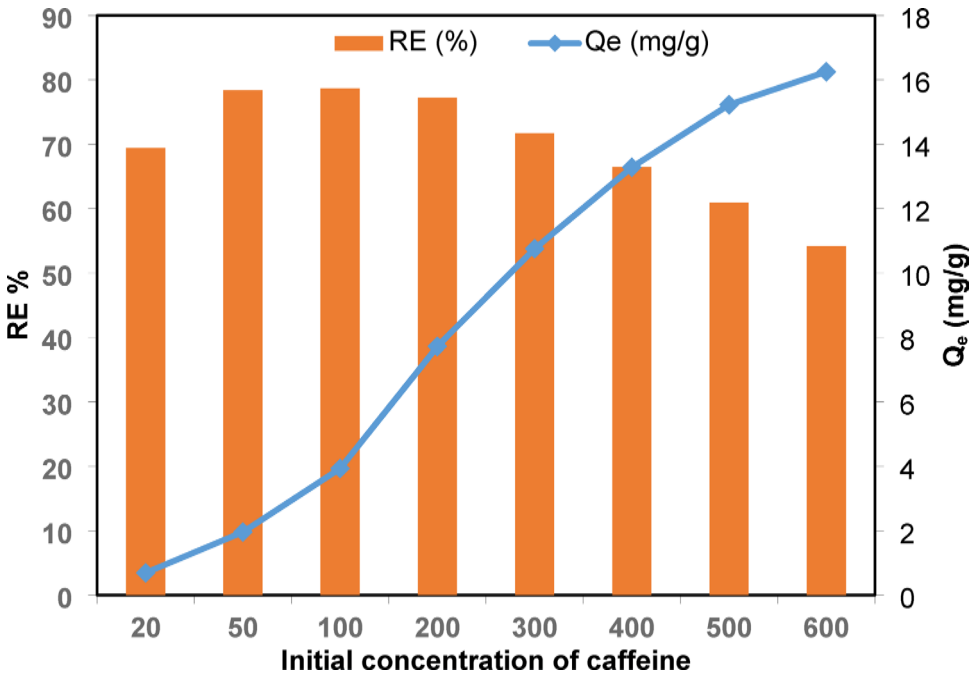

Fig. 7 Effect of initial concentration of caffeine. Experimental conditions: dosage of adsorbent (20 g/L), initial concentration (20–600 mg/L) of caffeine, temperature (298 K), agitation speed (100 rpm) and contact time (1 h)

Table 3 Langmuir, Freundlich and Temkin adsorption isotherm parameters for the adsorption of caffeine on AC-K

Model	Equation	Parameters	Value
Langmuir	$Q_e = \frac{Q_{max} * K_L * C_e}{1 + K_L * C_e}$	Q_{max} (mg/g)	22.02
		K_L (L/g)	0.011
		R^2	0.996
		RSME	0.353
Freundlich	$Q_{e=K_F} C_e^{1/n}$	K_F.(mg/g)(L/mg)$^{1/n}$	0.916
		n	1.896
		R^2	0.951
		RSME	1.772
Temkin	$Q_e = \frac{RT}{b} \ln(K_T C_e)$	b (J/mol)	4.342
		K_T (L/g)	0.149
		R^2	0.987
		RMSE	0.638

Where Q_{max} (mg/g) is the adsorbent's maximum monolayer adsorption capacity, *Ce* (mg/L) is concentration of adsorbate at equilibrium, q_e is the adsorption capacity at equilibrium, K_L is the Langmuir constant which is related to free energy of adsorption (L/mg), K_F is the Freundlich constant which indicates adsorption capacity (mg/g), *n* is the adsorption intensity (dimensionless), K_T is the Temkin constant (L/g), b is the heat of adsorption (J/mol), T is the absolute temperature (K) and R is the universal gas constant (8.314 J mol^{-1} K^{-1})

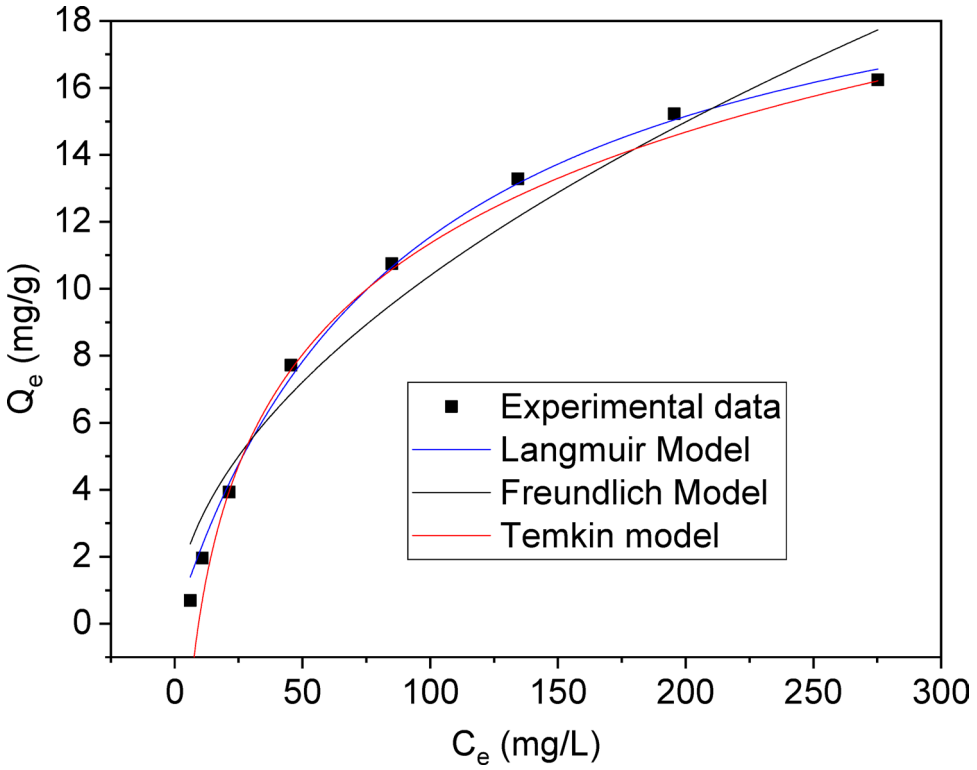

Fig. 8 Langmuir, Freundlich and Temkin isothermal models. Experimental conditions: dosage of adsorbent (20 g/L), initial concentration (20–600 mg/L), temperature (25 °C), agitation speed (100 rpm) and contact time (1 h)

$$RMSE = \sqrt{\frac{1}{n}\sum_{i=1}^{n}\left(q_{e,exp} - q_{e,pred}\right)^2} \quad (3)$$

where $q_{e,exp}$, experimental adsorption capacity value, $q_{e,pred}$ predicted adsorption capacity value from the model, and *n* is the number of data points.

Adsorption kinetics

The kinetics of caffeine adsorption onto AC-K were investigated by monitoring uptake over time intervals ranging from 0 to 300 min. To elucidate the adsorption mechanism and rate-controlling steps, experimental kinetic data were analyzed using nonlinear regression using four kinetic models (as detailed in Table 4). Among these, the pseudo-second-order (PSO) model provided the most relevant fits for this system, as shown in Table 4 and Fig. 9. The nonlinear

Table 4 Kinetics parameters for the adsorption of caffeine on AC-K

Kinetic model	Equation	Parameter	Value
Pseudo-first order	$Q_{t=}Q_e(1-e^{-k_1 t})$	R^2	0.911
		Q_e (mg/g)	7.002
		Q_e (mg/g)	7.392
		k_1 (s^{-1})	0.14594
		RMSE	0.108
Pseudo-second order	$Q_t = \frac{Q_e^2 k_2 t}{1+Q_e k_2 t}$	R^2	0.995
		Q_e^* (mg/g)	7.454
		Q_e (mg/g)	7.392
		k_2 (L mol^{-1} s^{-1})	0.03204
		RMSE	0.017
Elovich	$Q_{t=}\frac{1}{\beta}\ln(\alpha\beta t+1)$	R^2	0.883
		α (mg/g)	26.329
		β (mg/g)	1.312
		RMSE	0.930
Weber's intraparticle diffusion	$Q_t = k_{diff}\times t^{1/2}+C$	R^2	0.618
		k_{diff} (mg g^{-1} $min^{-1/2}$)	0.218
		C (mm)	4.537
		RMSE	7.154

Where Q_e is the amount adsorbate adsorbed at equilibrium (mg/g), Q_t is the amount of adsorbate adsorbed at any time (mg/g), t is the adsorption time (min), α is the initial adsorption rate (mg/g min), β is desorption constant, which is related to the surface coverage and activation energy of chemisorption (mg/g), k_{diff} is the intraparticle diffusion rate constant (mg g^{-1} $min^{-1/2}$) and C is the thickness of boundary layer (mm), k_1 is the first rate constant (s^{-1}) and k_2 is the second rate constant (L mol^{-1} s^{-1})

regression analysis yielded correlation coefficients (R^2) of 0.911 for the PFO model, 0.995 for the PSO model, 0.883 for the Elovich model and 0.618 for Weber's intraparticle diffusion model. The exceptionally high R^2 value for the PSO model, very close to 1 (0.995), strongly indicates that the adsorption of caffeine onto AC-K predominantly follows PSO kinetics. Additionally, the determined root mean square error (RMSE) value for PSO was lower (0.017) compared to those of PFO (0.108), Elovich (0.930) and Weber's intraparticle diffusion (7.154). The dominance of PSO kinetics suggests that the overall adsorption rate is proportional to the square of the availlable adsorption sites or adsorbate concentration. This finding aligns with previous research on the adsorption kinetics of organic contaminants, such as phenol and methylene blue, onto activated carbons derived from non-woody waste biomass (Thithai et al. 2025).

Comparative study

The caffeine adsorption performance of AC-K from aqueous solutions was compared with other adsorbents based on adsorption capacity and removal efficiency (Table 5). AC-K achieved a maximum adsorption capacity of 22.02 mg/g and 78.67% removal efficiency. The observed performance of AC-K is lower than that of the activated carbon/alginate (ACA) (725.05 mg/g, 97.32%) and coconut leaf-derived AC (73.13 mg/g). The observed higher performance could be attributed to their larger surface areas of 678.03 m^2/g and 720 m^2/g for AC from coconut leaf, and activated carbon/alginate (ACA), respectively. AC-K with the surface area of 407.645 m^2/g demonstrates superior adsorption capacity (22.02 mg/g) compared to some adsorbents, such as oxidized pine needle biochar (6.26 mg/g), *fique bagasse* biochar (9.129 mg/g), and engineered tea-waste biochar (15.4 mg/g). The observations indicate that AC-K is a potential adsorbent for removing caffeine and related organic pollutants from aqueous solutions.

Optimization of adsorption process using RSM model

Box–Bohnken design

Response surface methodology (RSM) was implemented using Design-Expert® Software Version 13 to optimize adsorption conditions via a Box–Bohnken design (BBD), with experimental parameters detailed in Table 6. The BBD approach evaluates the interactive effects of multiple factors on adsorption performance. Four variables examined were solution pH, caffeine initial concentration, adsorbent dosage, and adsorption time. The experimental matrix comprised 29 randomized runs (Table 7), assessing AC-K's caffeine removal efficiency across variable combinations, presenting both actual and predicted outcomes (Table 7). The results demonstrated significant response variation, with removal efficiencies ranging from 30.04 to 90.40% for actual outcomes, and from 28.95 to 91.88% for predicted outcomes.

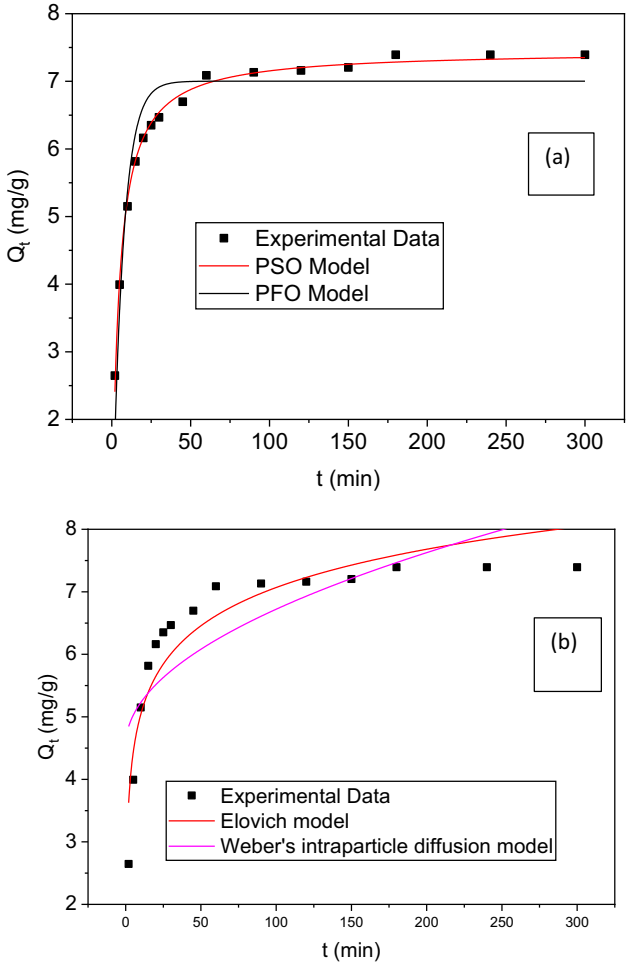

Fig. 9 Kinetics for the adsorption of caffeine on AC-K

ANOVA analysis

Analysis of variance (ANOVA) was employed to evaluate the influence of independent variables on the performance of the fitted quadratic polynomial model describing caffeine removal by AC-K (Table S2). The results demonstrate the model's high statistical significance. An exceptionally high model F-value of 241.06 for removal efficiency indicates a robust model, with only a 0.01% probability that this value could arise from random noise. The very low regression p value (<0.0001) further confirms the model's significance. Among the 14 model terms, 11 model terms were statistically significant ($p<0.05$): B, C, AB, AC, AD, BC, BD, CD, A^2, B^2, C^2, and D^2. The remaining three model terms (A, D, and CD) were excluded from the final model equation because they were insignificant ($p>0.05$). The selective retention of significant terms in the equation enhances the model's predictive capability and theoretical relevance. A similar finding was previously reported (Ambarita et al. 2023).

Model validity was further confirmed through diagnostic metrics (Tables S2 and S3). The lack of fit F-value (2.33) was not significant relative to pure error ($p=0.2105$), indicating a 21.05% probability that it could result from noise. The observed non-significant lack of fit is desirable, confirming that the model adequately describes the experimental data. Additionally, the close agreement between predicted R^2 (0.9786) and adjusted R^2 (0.9917) with a difference of only 0.0131 (<0.2) supports model adequacy. This similar results was previously observed (Grich et al. 2025). The Adeq precision value of 51.362, substantially exceeding the threshold of 4, indicates a strong signal-to-noise ratio.The similar finding was previously reported (Ayele et al. 2022).

Table 6 The Box Bohnken design (BBD) of independent variables for the adsorption of caffeine

Variables	Unit	Symbols	Level of variables		
			−α	0	+α
Solution pH		A	2	5	8
Concentration of caffeine	mg/L	B	20	60	100
Dosage of adsorbent	g/L	C	2	11	20
Adsorption time	min	D	5	62.5	120

Table 5 Caffeine adsorption capacity of different adsorbents

Adsorbent materials	Kinetic and isothermal model	Surface area (m^2/g)	Dosage and initial concentration	pHpzc of adsorbent	Solution pH	q_{max} (mg/g)	RE %	References
AC from coconut leaves	PSO Redlich-Peterson	678.03	–	7.9	4	73.13	–	Oliveira et al. (2022)
Ficus Benjamina zero-valent iron/copper nanoparticles	PSO Langmuir	–	0.2 g/L 5 mg/L	–	5	34.34	86	Abdel-Aziz et al. (2020)
Oxidized biochar obtained from pine needles	PSO Freundlich and Langmuir	–	–	–	4	6.26	–	Anastopoulos et al. (2020)
Fique Bagasse Biochar	Freundlich, Langmuir and Redlich-Peterson	–	–	–	6	9.129	–	Correa et al. (2019)
Activated carbon/alginate (ACA)	PSO Freundlich and Langmuir	790	0.1 g 0.5 mg/L	–	7	725.05	97.32	Mahgoub et al. (2024)
Engineered tea-waste biochar	Freundlich and Temkin	576.09	1 g/L 50 mg/L	–	3.5	15.4	–	Keerthanan et al. (2020)
AC from FPAA (AC-K)	PSO Langmuir	407.645	20 g/L 100 mg/L	6.0	7	22.02	78.67	This study

Table 7 Design matrix and response value for both actual and expected values for the adsorption of caffeine

Run	Factor 1 A: pH	Factor 2 B: Initial concentration (mg/L)	Factor 3 C: Adsorbent dosage (g/L)	Factor 4 D: Adsorption time (min)	Response efficiency %	
					Actual	Predicted
1	2	20	11	62.54	52.41	52.15
2	2	60	11	120	85.82	84.30
3	5	100	2	62.5	30.04	28.95
4	5	20	11	5	57.31	59.11
5	5	100	20	62.5	87.48	86.81
6	8	60	20	62.5	77.22	77.88
7	2	60	20	62.5	90.4	91.88
8	5	60	20	5	87.76	87.95
9	5	60	20	120	86.64	86.27
10	8	100	11	62.5	59.87	61.43
11	5	20	11	120	65.94	67.90
12	8	60	2	62.5	49.13	48.72
13	5	20	2	62.5	36.06	34.37
14	5	60	11	62.5	87.38	86.84
15	5	60	11	62.5	86.5	86.84
16	8	20	11	62.5	70.93	70.40
17	5	60	2	5	41.77	43.44
18	8	60	11	5	82.46	81.62
19	5	20	20	62.5	61.1	59.83
20	8	60	11	120	78.23	77.79
21	5	60	11	62.5	85.01	86.84
22	5	60	11	62.5	88.31	86.84
23	5	60	11	62.5	87.01	86.84
24	2	60	2	62.5	37.31	37.72
25	5	60	2	120	46.37	47.47
26	2	60	11	5	80.04	78.11
27	5	100	11	120	71.8	71.07
28	5	100	11	5	78.39	77.50
29	2	100	11	62.5	80.85	82.68

Based on this analysis, the significant terms were used to develop the final quadratic polynomial model (Eq. 4). This equation quantifies the impact of independent variables on caffeine removal efficiency: Positive coefficients indicate a favorable effect on adsorption capacity, while negative coefficients denote an inhibitory effect. The model provides a statistically validated mathematical framework for optimizing and interpreting the adsorption process.

$$\begin{aligned}\text{Removal efficiency} = {} & 86.84 - 0.7492\text{A} + 5.39\text{B} \\ & + 20.83\text{C} + 0.5892\text{D} - 9.87\text{AB} \\ & - 6.25\text{AC} - 2.50\text{AD} + 8.1\text{BC} \\ & - 3.80\text{BD} - 1.43\text{CD} - 4.31\text{A}^2 \\ & - 15.87\text{B}^2 - 18.48\text{C}^2 - 2.08\text{D}^2\end{aligned} \quad (4)$$

Figure S3a compares the predicted removal efficiency (RE %) from the regression model against the experimental values. The close alignment of data points along the 1:1 line demonstrates a strong linear relationship, confirming the model's ability to accurately predict experimental outcomes. Figure S3b presents the residual analysis used to assess model accuracy. The residuals exhibit a normal distribution pattern with no significant outliers or discernible patterns in their variance. This indicates the model's assumptions regarding error structure are valid. Figure S3c further validates the model by plotting the external Studentized residuals for each experimental run. All residuals fall within the critical range of ±3, confirming the absence of significant outliers or influential data points. The diagnostic plots (Fig. S3a–c) support the robustness and validity of the developed quadratic model.

Effect of independent variables

Four independent variables (pH, initial caffeine concentration, adsorbent dosage, and contact time) were evaluated for their effect on adsorption efficiency. The response surface methodology visualized these effects through 3D surface plots and contour diagrams (Fig. 10, each pairing two variables while maintaining others at constant levels. These plots illustrate interactive effects by displaying independent variables on orthogonal axes (x_1, x_2) with removal efficiency

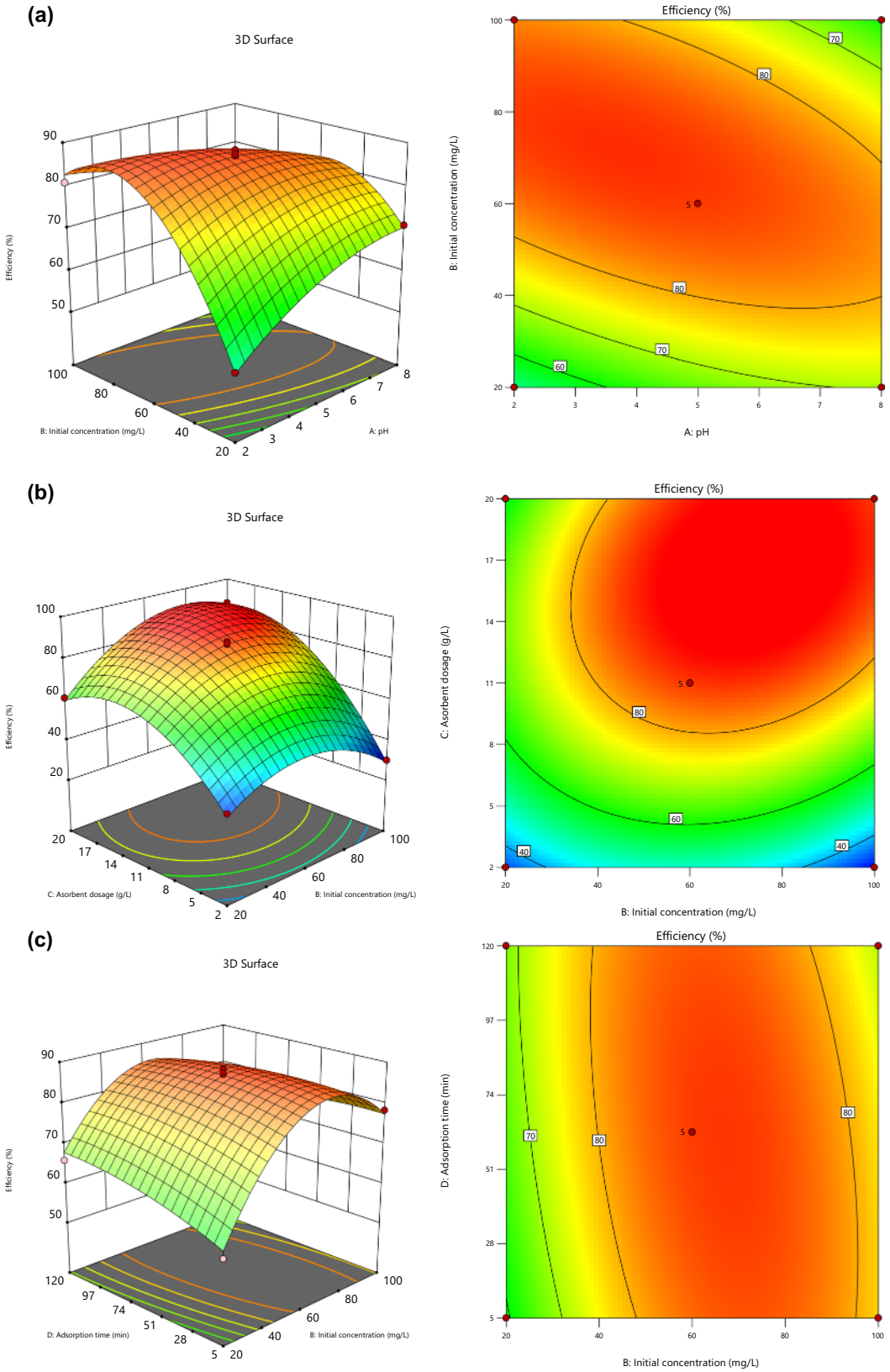

Fig. 10 The interaction of two different independent variables for the adsorption of caffeine, 3D plots (left) and Contour (right)

on the z-axis (3D) or through iso-response lines (contours), enabling comprehensive analysis of variable interactions on caffeine adsorption performance.

Effect of initial concentration and pH The influence of initial caffeine concentration and solution pH on adsorption efficiency by AC-K is presented in Fig. 10a. The removal efficiency initially increased proportionally with rising caffeine concentration up to 60 mg/L and solution pH up to 5. Under these conditions, the maximum removal efficiency of 87% was achieved. However, further increases beyond these optimal points resulted in a decline in the removal efficiency. At concentrations exceeding 60 mg/L, the available adsorption sites on AC-K likely approached saturation, reducing the efficiency increment per unit concentration increase. This positive trend can be attributed to the enhanced driving force for mass transfer at higher concentrations and the likely optimization of interactions between the caffeine molecules (neutral at pH 3–8) and the AC-K surface (positively charged) at pH 5). The interactions of AC-K with caffeine at the pH range 3–8 are mainly based on pore filling, π–π-interactions, and hydrogen bonding with no electrostatic interaction. The dissimilar finding was previously reported, where removal efficiency increased as the initial concentration of caffeine was also increased, with less impact of pH for caffeine removal using *Elaeis guineensis* AC (Melo et al. 2020). The study similarly identified optimal conditions (specific concentration and pH) maximizing removal, beyond which efficiency decreased, underscoring the general importance of optimizing these parameters for efficient contaminant removal using activated carbons. The consistency between these systems highlights the critical role of adsorbate speciation, adsorbent surface charge, and site saturation in determining adsorption performance.

Effect of adsorbent dosage and initial concentration Adsorbent dosage and initial caffeine concentration significantly influence adsorption efficiency. As shown in Fig. 10b, increasing either the dosage or the initial concentration leads to higher caffeine removal efficiency. This interaction likely occurs because a higher adsorbent dosage provides more available adsorption sites, while a higher initial concentration increases the number of adsorbate molecules available for attachment. These factors enhance the probability of caffeine molecules encountering and binding to active sites. Similar findings have been reported for the decolourization of Blue 19 using *Dictyota bartayresiana* biosorbent (Geethamala et al. 2025).

Effect of adsorption time and initial concentration Adsorption time and initial caffeine concentration both influence adsorption efficiency, as shown in Fig. 10c. The caffeine removal efficiency increases with higher initial concentrations, reaching an optimum of 87% at 62.5 min and 60 mg/L. However, as concentration exceeds 60 mg/L, removal efficiency decreases. The adsorption time shows no effect on caffeine removal using AC-K. This is demonstrated by two key observations varying initial concentration (at any fixed time) directly alters removal efficiency, while at a near-constant initial concentration (~60 mg/L), efficiency remains essentially unchanged across the entire tested time range (5–120 min). This time-independent behavior contrasts with the adsorption of Rhodamine B onto AC from *Delonix regia* Seeds and Pods, where efficiency increased continuously with time until equilibrium was reached (Azeez et al. 2022b).

Proposed adsorption mechanism

The adsorption of caffeine was proposed to involve multiple interactions, as shown in Fig. 11. The oxygenated surface of AC offers numerous active sites capable of forming hydrogen bonds. Caffeine molecules also contain heteroatoms (nitrogen and oxygen) within amide, amine, and carbonyl groups that allow them to participate in hydrogen bonding. Additionally, AC-K and caffeine possess conjugated aromatic ring systems with delocalized π-electrons. The interaction between these π-electron clouds arises from electrostatic forces, including quadrupole–quadrupole interactions, as well as London dispersion forces. These π–π interactions promote the association of caffeine molecules with the graphitic basal planes of AC-K. Additionally, Van Der Waals forces such as London dispersion forces and dipole–dipole interactions contribute significantly to the adsorption process between adsorbent and caffeine molecules (Mukherjee et al. 2024). The presence of oxygen and nitrogen atoms in caffeine, along with similar heteroatoms on the AC-K surface, generates regions of partial positive and partial negative charges. These charge distributions facilitate dipole–dipole attractions. London dispersion forces further arise from temporarily induced dipoles formed between adjacent atoms of caffeine and the AC-K surface. Therefore, the caffeine adsorption onto AC-K is a synergistic process rather than a single, isolated mechanism. Hydrogen bonding, dipole–dipole interactions, London

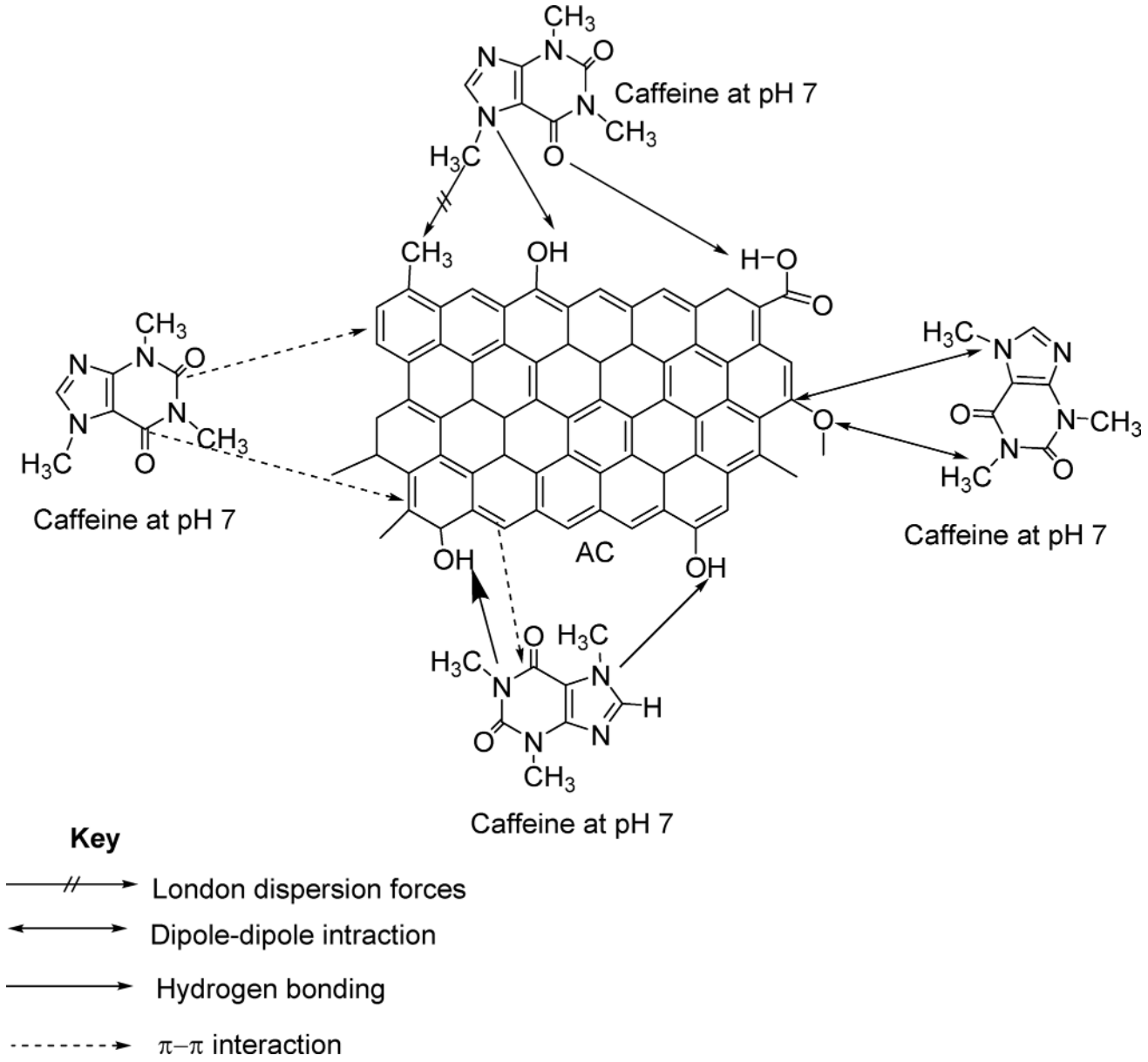

Fig. 11 A proposed adsorption mechanism of caffeine on AC-K

dispersion forces, and π–π interactions collectively determine the overall adsorption behavior of caffeine.

Conclusions

This study demonstrated that activated carbon (AC-K) derived from *A. angustifolium* fruit shells is a sustainable adsorbent for the removal of caffeine from aqueous solutions. The activated carbon prepared using KOH activating agent and pyrolysis at 500ºC exhibited increased pore surface area, pore diameter and pore volume. A maximum adsorption capacity of 22.02 mg/g was obtained using pH 7, 20 g/L AC-K dosage, 20–600 mg/L initial caffeine concentration, 25 °C temperature, 100 rpm agitation speed, and 1 h adsorption time. The Langmuir isotherm and pseudo-second-order kinetic model best described the adsorption behavior of caffeine. Thus, the adsorption of caffeine molecules formed a monolayer film that was adsorbed on the surface of AC-K using multiple interactions. The results from this study suggest that the shells from *A. angustifolium* fruit is a potential precursor for producing activated carbon suitable for the removal of emerging contaminants such as caffeine and related chemicals from aqueous solutions.

Supplementary Information The online version contains supplementary material available at https://doi.org/10.1007/s11696-0

26-04973-5.

Acknowledgements The authors thank Mr. Mpeji Ndabuli and Mis. Aneth Coster from the Department of Chemistry and Physics (SUA) for their technical assistance during the conduct of experiments and Dr. Magori Nyangi of the Water Institute, Dar es Salaam, Tanzania, for his assistance on the use of Design Expert Software.

Author contributions All authors have accepted responsibility for the entire content of this manuscript and consented to its submission to the journal, reviewed all the results and approved the final version of the manuscript. B.A.K. conceptualization, methodology, formal analysis, investigation, writing original draft preparation. A.J.M and E.S.L. conceptualization, methodology, investigation, review and editing.

Funding Sokoine University of Agriculture (SUA) funded the study.

Data availability The datasets generated during and/or analysed during the current study are available from the corresponding author on reasonable request.

Declarations

Conflict of interest The authors declare no competing interests.

Ethical approval Not applicable.

Consent to participate Not applicable.

Consent for publication Not applicable.

References

Abdel-Aziz MH, Farag R, Abdel-Gawad S (2020) Removal of caffeine from aqueous solution by green approach using *Ficus benjamina* zero-valent iron/copper nanoparticles. Adsorpt Sci Technol 38:026361742094749. https://doi.org/10.1177/02636174209474 95

Abdulsalam A, Le TPP, Nguyen TS, Ali JK, Abubasha MY, Jouini MS et al (2025) A review of fouling prediction techniques in membrane desalination: from empirical to intelligent models. Desalination 616:119363. https://doi.org/10.1016/j.desal.2025.119363

Adetokun A, Uba S, Garba Z (2018) Optimization of adsorption of metal ions from a ternary aqueous solution with activated carbon from *Acacia senegal* (L.) willd pods using central composite design. J King Saud Univ Sci 31:1452–1462. https://doi.org/10.1016/j.jksus.2018.12.007

Alawa B, Singh S, Chakma S, Kishor R, Stålsby Lundborg C, Diwan V (2025) Development of novel biochar adsorbent using agricultural waste biomass for enhanced removal of ciprofloxacin from water: insights into the isotherm, kinetics, and thermodynamic analysis. Chemosphere 375:144252. https://doi.org/10.1016/j.chemosphere.2025.144252

Ambarita AC, Arahman N, Bilad MR, Gül BY, Korkut S, Yüksekdağ A et al (2023) Polyethersulfone membrane coated with Dragon blood resin: effect of input parameters and optimization using response surface methodology. S Afr J Chem Eng 45:30–41. https://doi.org/10.1016/j.sajce.2023.04.005

Anastopoulos I, Katsouromalli A, Pashalidis I (2020) Oxidized biochar obtained from pine needles as a novel adsorbent to remove caffeine from aqueous solutions. J Mol Liq 304:112661. https://doi.org/10.1016/j.molliq.2020.112661

Asiain-Mira R, Zamora P, Monsalvo V, Torrente-Murciano L (2024) Effect of functional groups on the adsorption of urea on activated carbon. Carbon 228:119361. https://doi.org/10.1016/j.carbon.2024.119361

Ayele AL, Tizazu BZ, Wassie ABJAS (2022) Chemical modification of teff straw biomass for adsorptive removal of Cr (VI) from aqueous solution: characterization, optimization, kinetics, and thermodynamic aspects. Adsorpt Sci Technol. https://doi.org/10.1155/2022/5820207

Azeez S, Jimoh A, Saheed I, Otun K, Mustapha O, Adekola F (2022a) Optimization by Box Behnken design for eosin yellow dye removal from aqueous medium using date palm seeds-porous carbon@TiO_2 blend. J Niger Soc Phys Sci 4:183–192. https://doi.org/10.46481/jnsps.2022.533

Azeez S, Saheed I, Adekola F, Jimoh A, Aransiola D, Abdulsalam Z (2022b) Box Behnken Design in the optimization of Rhodamine B adsorption onto activated carbon prepared from *Delonix regia* seeds and pods. J Turk Chem Soc A Chem 9:205–222. https://doi.org/10.18596/jotcsa.893472

Babuponnusami A, Sinha S, Ashokan H, Veliyath M, Hariharan S, Jayaseelan A et al (2023) Advanced oxidation process (AOP) combined biological process for wastewater treatment: a review on advancements, feasibility and practicability of combined techniques. Environ Res 237:116944. https://doi.org/10.1016/j.envres.2023.116944

Bahrami M, Amiri MJ, Koochaki SJP (2017) Removal of caffeine from aqueous solution using multi-wall carbon nanotubes: kinetic, isotherm, and thermodynamics studies. Pollution 3(4):539–552. https://doi.org/10.22059/POLL.2017.62771

Banerjee S, Chattopadhyaya MC (2017) Adsorption characteristics for the removal of a toxic dye, tartrazine from aqueous solutions by a low cost agricultural by-product. Arab J Chem 10:S1629–S1638. https://doi.org/10.1016/j.arabjc.2013.06.005

Chagu J, Mwakalesi AJ (2026) Effects of phosphoric acid concentration on properties of activated carbon from *Strychnos spinose* fruit shells. Sci Rep 16(1):4009. https://doi.org/10.1038/s41598-025-34098-w

Clayman CL, Connaughton VP (2022) Neurochemical and behavioral consequences of ethanol and/or caffeine exposure: effects in zebrafish and rodents. Curr Neuropharmacol 20(3):560–578. https://doi.org/10.2174/1570159x19666211111142027

Correa Y, Giraldo L, Moreno-Piraján J (2019) Caffeine adsorption by fique bagasse biochar produced at various pyrolysis temperatures. Oriental J Chem 35:538

Dao TM, Le Luu T (2020) Synthesis of activated carbon from macadamia nutshells activated by H_2SO_4 and K_2CO_3 for methylene blue removal in water. Bioresour Technol Rep 12:100583. https://doi.org/10.1016/j.biteb.2020.100583

Durak H, Yarbay RZ, Atilgan Türkmen B (2026) Hydrothermal carbonization of biomass for hydrochar production: mechanisms, process parameters, and sustainable valorization. Processes 14(2):339

Fonseca-Bermúdez ÓJ, Giraldo L, Sierra-Ramírez R, Serafin J, Dziejarski B, Bonillo MG et al (2024) Cashew nut shell biomass: a source for high-performance CO_2/CH_4 adsorption in activated carbon. J CO2 Util 83:102799. https://doi.org/10.1016/j.jcou.2024.102799

Geethamala G, Swathilakshmi A, Poonkothai M (2025) Dictyota bartayresiana a sustainable biosorbent for the decolorization of reactive blue 19—optimization, equilibrium, desorption and toxicological studies. Bioremediat J. https://doi.org/10.1080/10889868.2025.2453734

Grich A, Naboulsi A, Bouzid T, Yazid H, Elbasraoui A, Regti A et al (2025) Doum fiber-derived activated carbon via H_3PO_4-assisted pyrolysis for sulfamethoxazole removal: Box-Behnken design

optimization and mechanistic approach. Diamond Relat Mater 156:112464. https://doi.org/10.1016/j.diamond.2025.112464
Guan Z-L, Wang Y-D, Wang Z, Hong Y, Liu S-L, Luo H-W et al (2024) The synthesis, characteristics, and application of hierarchical porous materials in carbon dioxide reduction reactions. Catalysts 14(12):936
Ibrahim A, Ismail A, Juahir H, Ovinis M, Ihsan YN, Sudianto S et al (2024) BTEX adsorption from aqueous solutions using activated carbon from *Melaleuca cajuputi* leaves. Kuwait J Sci 51(4):100247. https://doi.org/10.1016/j.kjs.2024.100247
Kasazi BA, Mwakalesi AJ, Lema ES (2026) Efficient and reusable activated carbon from *Aframomum angustifolium* fruits' shells for removal of Ceftriaxone from aqueous solution: Adsorption isotherms, kinetics, and thermodynamics studies (*Aframomum angustifolium*; biowaste; activated carbon; Ceftriaxone; antibiotic). Indones J Chem 26(2):17. https://doi.org/10.22146/ijc.108042
Keerthanan S, Bhatnagar A, Mahatantila K, Jayasinghe C, Ok YS, Vithanage M (2020) Engineered tea-waste biochar for the removal of caffeine, a model compound in pharmaceuticals and personal care products (PPCPs), from aqueous media. Environ Technol Innov 19:100847. https://doi.org/10.1016/j.eti.2020.100847
Korekar G, Kumar A, Ugale C (2020) Occurrence, fate, persistence and remediation of caffeine: a review. Environ Sci Pollut Res 27(28):34715–34733. https://doi.org/10.1007/s11356-019-06998-8
Kouhi K, Amouei A, Asgharnia H, Vosoughi Niri M, Fallah S, Shirmardi M (2023) Application of oak charcoal-based activated carbon for the removal of methylene blue dye from aqueous solutions: kinetics, equilibrium, and reusability studies. Water Pract Technol 18:3255–3270. https://doi.org/10.2166/wpt.2023.203
Kumagai S, Sato M, Tashima D (2013) Electrical double-layer capacitance of micro- and mesoporous activated carbon prepared from rice husk and beet sugar. Electrochim Acta 114:617–626. https://doi.org/10.1016/j.electacta.2013.10.060
Kyayesimira J, Mawanda I, Andama M, Safari D (2019) Studies on the utilization and proximate composition of wild *Aframomum anguistifolium* (sonn.) K. Schum fruits in Nakaseke district, Uganda. Afr J Food Agric Nutr Dev 19:14790–14804. https://doi.org/10.18697/ajfand.87.17605
Lee H, Fiore S, Berruti F (2024) Adsorption of methyl orange and methylene blue on activated biocarbon derived from birchwood pellets. Biomass Bioenergy 191:107446. https://doi.org/10.1016/j.biombioe.2024.107446
Li S, He B, Wang J, Liu J, Hu X (2020a) Risks of caffeine residues in the environment: necessity for a targeted ecopharmacovigilance program. Chemosphere 243:125343. https://doi.org/10.1016/j.chemosphere.2019.125343
Li S, Wen J, He B, Wang J, Hu X, Liu J (2020b) Occurrence of caffeine in the freshwater environment: implications for ecopharmacovigilance. Environ Pollut 263:114371. https://doi.org/10.1016/j.envpol.2020.114371
Mahgoub SM, Kotp AA, Mohamed MA, Alfassam HE, Rudayni HA, Allam AA et al (2024) Assessment of activated carbon/alginate for the concurrent removal efficiency of paracetamol and caffeine from wastewater in their binary solutions. Chin J Anal Chem 52(7):100403. https://doi.org/10.1016/j.cjac.2024.100403
Megherbi H, Runtti H, Tuomikoski S, Heponiemi A, Hu T, Lassi U et al (2025) The effect of phosphoric acid on the properties of activated carbons made from *Myrtus communis* leaves: textural characteristics, surface chemistry, and capacity to adsorb methyl orange. J Mol Struct 1321:140038. https://doi.org/10.1016/j.molstruc.2024.140038
Melliti A, Touihri M, Kofroňová J, Hannachi C, Sellaoui L, Bonilla-Petriciolet A et al (2024) Sustainable removal of caffeine and acetaminophen from water using biomass waste-derived activated carbon: synthesis, characterization, and modelling. Chemosphere 355:141787. https://doi.org/10.1016/j.chemosphere.2024.141787
Melo LLA, Ide AH, Duarte JLS, Zanta C, Oliveira L, Pimentel WRO et al (2020) Caffeine removal using *Elaeis guineensis* activated carbon: adsorption and RSM studies. Environ Sci Pollut Res 27(21):27048–27060. https://doi.org/10.1007/s11356-020-09053-z
Minakshi M, Mujeeb A, Whale J, Evans R, Aughterson R, Shinde P et al (2024) Synthesis of porous carbon honeycomb structures derived from hemp for hybrid supercapacitors with improved electrochemistry. ChemPlusChem 89:e202400408. https://doi.org/10.1002/cplu.202400408
Miotto A, Orchulhak A, Enzweiler H, Paulino A, Visioli L (2024) Caffeine removal from water using rice husk residue biochar: characterization, kinetics and sorption isotherms. Int J Environ Sci Technol 22:7197–7210. https://doi.org/10.1007/s13762-024-06086-6
Mohite D, Dubal S, Lokhande P, Kadam V, Jagtap C, Rednam U et al (2024) Electrochemical evaluation of ZnO and PAN-based carbon nanofibers composite for high-performance supercapacitor application. Ionics 30:8469–8480. https://doi.org/10.1007/s11581-024-05869-8
Mpaka LJ, Mwakalesi AJ (2025) Adsorption kinetics of picloram on chitosan-modified *Strychnos pungens* fruit shell activated carbon. React Kinet Mech Catal. https://doi.org/10.1007/s11144-025-02973-2
Mukherjee S, Borah PP, Bhattacharyya K, Biswas S (2024) Post-synthetically modified cationic, robust MOF featuring selective separation of carboxylate-containing pharmaceutical drugs from water at neutral pH: elucidation of the adsorption mechanism by theory and experiments. Inorg Chem 63(33):15421–15432. https://doi.org/10.1021/acs.inorgchem.4c02439
Nandi R, Jha MK, Guchhait SK, Sutradhar D, Yadav S (2023) Impact of KOH activation on rice husk derived porous activated carbon for carbon capture at flue gas alike temperatures with high CO2/N2 selectivity. ACS Omega 8(5):4802–4812. https://doi.org/10.1021/acsomega.2c06955
Neolaka YAB, Riwu AAP, Aigbe UO, Ukhurebor KE, Onyancha RB, Darmokoesoemo H et al (2023) Potential of activated carbon from various sources as a low-cost adsorbent to remove heavy metals and synthetic dyes. Results Chem 5:100711. https://doi.org/10.1016/j.rechem.2022.100711
Oliveira EN, Meneses AT, de Melo SF, Dias FMR, Perazzini MTB, Perazzini H et al (2022) Highly effective adsorption of caffeine by a novel activated carbon prepared from coconut leaf. Environ Sci Pollut Res Int 29(33):50661–50674. https://doi.org/10.1007/s11356-022-18788-w
Parmar K (2017) Biomass—an overview on composition characteristics and properties (biomass; categorization; composition; property). IRA InternationRA Int J Appl Sci 7(1):10. https://doi.org/10.21013/jas.v7.n1.p4
Pavia DL, Lampman GM, Kriz GS (2001) Introduction to organic spectroscopy, 3rd edn. Brooks Cole Publishers, Philadelphia, p 139
Phuoc N, Quoc H, Tran T, Tan L, Hoang B (2023) Optimization of ciprofloxacin removal by response surface methodology using activated carbon from Burmese grape obtained from Vietnam. J Chem Res. https://doi.org/10.1177/17475198231212143
Rahmawati A, Muthia D, Imelda M, Latief F, Mohamad S, Kiswandono A et al (2024) Removal of ceftriaxone and ciprofloxacin antibiotics from aqueous solutions using graphene oxide derived from corn cob. Glob J Environ Sci Manag 10(2):573–588
Ramutshatsha-Makhwedzha D, Mavhungu A, Moropeng ML, Mbaya R (2022) Activated carbon derived from waste orange and lemon peels for the adsorption of methyl orange and methylene blue

dyes from wastewater. Heliyon 8(8):e09930. https://doi.org/10.1016/j.heliyon.2022.e09930
Rathi BS, Kumar PS (2021) Application of adsorption process for effective removal of emerging contaminants from water and wastewater. Environ Pollut 280:116995. https://doi.org/10.1016/j.envpol.2021.116995
Rathinam A, Sree Nithi SV, Meili L, Chellam PV (2026) Persulfate-based oxidative degradation of simulated caffeinated aqueous solutions: machine learning integration and comparative model analysis. J Indian Chem Soc. https://doi.org/10.1016/j.jics.2026.102618
Reddy VS, Shiva S, Manikantan S, Ramakrishna S (2024) Pharmacology of caffeine and its effects on the human body. Eur J Med Chem Rep 10:100138. https://doi.org/10.1016/j.ejmcr.2024.100138
Rigueto CVT, Nazari MT, De Souza CF, Cadore JS, Brião VB, Piccin JS (2020) Alternative techniques for caffeine removal from wastewater: an overview of opportunities and challenges. J Water Process Eng 35:101231. https://doi.org/10.1016/j.jwpe.2020.101231
Rodrigues S, Alves RS, Antunes SC (2025) Impact of caffeine on aquatic ecosystems: assessing trophic-level biological responses. J Xenobiot. https://doi.org/10.3390/jox15030086
Rzyska-Szczupak K, Przybylska-Balcerek A, Buśko M, Szwajkowska-Michałek L, Szablewski T, Stuper-Szablewska K (2025) Roasting temperature as a factor modifying the caffeine and phenolic content of Ethiopian coffee. Processes 13(7):2037
Saghir Y, Chaoui A, Farsad S, Ben Hamou A, Amjlef A, Benafqir M et al (2025) Improving the adsorption efficiency of a low-cost natural adsorbent for the removal of an organic pollutant: optimization and mechanism study. Mater Adv 6(14):4857–4873. https://doi.org/10.1039/D5MA00253B
Samoggia A, Rezzaghi T (2021) The consumption of caffeine-containing products to enhance sports performance: an application of an extended model of the theory of planned behavior. Nutrients. https://doi.org/10.3390/nu13020344
Sharma G, Sharma S, Kumar A, Lai C, Naushad M, Dr S et al (2022) Activated carbon as superadsorbent and sustainable material for diverse applications. Adsorpt Sci Technol 2022:1–21. https://doi.org/10.1155/2022/4184809
Sri Shalini S, Palanivelu K, Ramachandran A, Raghavan V (2021) Biochar from biomass waste as a renewable carbon material for climate change mitigation in reducing greenhouse gas emissions—a review. Biomass Convers Biorefinery 11(5):2247–2267. https://doi.org/10.1007/s13399-020-00604-5
Tan X, Liu Y, Zeng G, Wang X, Hu X, Gu Y et al (2015) Application of biochar for the removal of pollutants from aqueous solutions. Chemosphere 125:70–85. https://doi.org/10.1016/j.chemosphere.2014.12.058
Teixeira C, Rodrigues S, Amorim J, Diogo BS, Pinto I, Carvalho AP et al (2025) Comprehensive machine learning assessment of zebrafish behaviour and biochemical markers in response to caffeine exposure. Ecotoxicology 34(5):746–759. https://doi.org/10.1007/s10646-025-02873-0
Thithai V, Gim SM, Mearaj S, Choi JW (2025) Adsorption kinetics and capacity of activated carbon derived from non-woody waste biomass for water remediation. Int J Environ Sci Technol 22(2):693–706. https://doi.org/10.1007/s13762-024-05677-7
Tihay V, Gillard P (2010) Pyrolysis gases released during the thermal decomposition of three Mediterranean species. J Anal Appl Pyrolysis 88(2):168–174. https://doi.org/10.1016/j.jaap.2010.04.002
Toniciolli Rigueto C, Torres Nazari M, Favretto de Souza C, Cadore J, Brião V, Piccin J (2020) Alternative techniques for caffeine removal from wastewater: an overview of opportunities and challenges. J Water Process Eng 35:101231. https://doi.org/10.1016/j.jwpe.2020.101231
Tran H (2023) Adsorption technology for water and wastewater treatments. https://www.mdpi.com/books/book/7760
Tugume P, Research C (2020) Traditional use of wild edible plants in the communities adjacent to Mabira Central Forest Reserve, Uganda. Ethnobot Res Appl 20:1–14
Ullah S, Shah SSA, Altaf M, Hossain I, El Sayed ME, Kallel M et al (2024) Activated carbon derived from biomass for wastewater treatment: synthesis, application and future challenges. J Anal Appl Pyrolysis 179:106480. https://doi.org/10.1016/j.jaap.2024.106480
Valencia L, Rosas W, Aguilar-Sanchez A, Mathew AP, Palmqvist AEC (2019) Bio-based micro-/meso-/macroporous hybrid foams with ultrahigh zeolite loadings for selective capture of carbon dioxide. ACS Appl Mater Interfaces 11(43):40424–40431. https://doi.org/10.1021/acsami.9b11399
Yang Y, Wan Y, Chen H, Li Y, Muñoz-Carpena R, Huang J et al (2025) Caffeine removal in wastewater: a comprehensive review of current treatment plants and small-scale innovations. Environ Technol Rev 14:594–612. https://doi.org/10.1080/21622515.2025.2512483
Zhang W, Huang W, Tan J, Huang D, Ma J, Wu B (2023) Modeling, optimization and understanding of adsorption process for pollutant removal via machine learning: recent progress and future perspectives. Chemosphere 311:137044. https://doi.org/10.1016/j.chemosphere.2022.137044